

Inflationary Phase Transitions in the Early Universe: A Bayesian Study with Space-Based Gravitational Waves Detectors

Qingyuan Liang^{a,b} Chen Yang^{a,b,c} Haipeng An^{c,d} Huai-Ke Guo^{a,b}

^a*International Centre for Theoretical Physics Asia-Pacific (ICTP-AP), University of Chinese Academy of Sciences (UCAS), Beijing, China.*

^b*Taiji Laboratory for Gravitational Wave Universe (Beijing/Hangzhou), University of Chinese Academy of Sciences (UCAS), Beijing, China.*

^c*Department of Physics, Tsinghua University, Beijing 100084, China*

^d*Center for High Energy Physics, Tsinghua University, Beijing 100084, China*

E-mail: qingyuan211045@gmail.com, yangchen26@ucas.ac.cn,
anhp@mail.tsinghua.edu.cn, guohuaike@ucas.ac.cn

ABSTRACT: Phase transitions during inflation can generate a stochastic gravitational-wave background that probes primordial physics. We study the detectability and parameter reconstruction of such a signal with a space-based gravitational-wave detector. Using a Taiji-like mission as a benchmark, we construct a realistic data-analysis framework that includes instrumental noise, astrophysical foregrounds and backgrounds, and the A , E , and T time-delay interferometry channels. The target signal is described in a minimal, model-independent form and analyzed using both Fisher-matrix forecasts and Bayesian inference with nested sampling. We quantify detection significance and parameter-recovery thresholds, showing that while detection is achievable at moderate signal-to-noise ratios, stronger signals provide more reliable parameter reconstruction. These results offer a realistic assessment of the capability of future space-based missions to probe phase transitions during inflation through stochastic gravitational radiation.

Contents

1	Introduction	1
2	Gravitational Waves from Phase Transition during Inflation	3
3	Data Analysis Framework with Taiji	5
4	Results	7
5	Conclusion	11

1 Introduction

A stochastic gravitational-wave background (SGWB) of cosmological origin carries fossil information from the early Universe and provides a powerful observational window into physics at energy scales far beyond those accessible to terrestrial experiments [1–3]. Unlike transient gravitational-wave (GW) signals, a cosmological SGWB is generated by collective processes operating in the primordial plasma and is therefore sensitive to the thermal history and symmetry-breaking dynamics of the early Universe [4–6]. Recent reviews provide comprehensive discussions of the theoretical foundations and observational prospects of cosmological SGWBs [7]. Searches for the SGWB span a wide frequency range. In the nanohertz band, PTA experiments have reported evidence for a stochastic signal [8–11]. At higher frequencies, ground-based interferometers including Advanced LIGO, Virgo, and KAGRA operate in the audio band and have placed upper limits in the absence of a detection [12–16]. Space-based interferometers such as Taiji, LISA, and TianQin will probe the millihertz band [17–25].

Among the most promising cosmological mechanisms for generating an SGWB are first-order phase transitions (FOPTs) in the early Universe [26]. Extensive theoretical studies have shown that FOPTs can produce SGWB spectra with amplitudes and characteristic frequencies well suited for detection by space-based missions [26–30]. Moreover, phase transitions during inflation (InPTs) can generate GWs together with curvature perturbations, which in turn source scalar-induced GWs upon horizon reentry [31–34]. Unlike thermal phase transitions that occur during the radiation-dominated era, InPTs are vacuum phase transitions, in which both GWs and curvature perturbations arise solely from bubble collisions.

Although many phenomenological studies of phase-transition-induced SGWBs rely on signal-to-noise ratio (SNR) estimates derived from sensitivity curves, extracting a weak

cosmological signal from realistic space-based data remains challenging [35]. In practice, the SGWB must be disentangled not only from instrumental noise but also from stochastic astrophysical components, including the confusion foreground produced by unresolved Galactic binaries and the background generated by extragalactic compact binary coalescences [36–38]. A realistic assessment of detectability therefore requires a statistical framework that simultaneously models all relevant components and their correlations [39].

Space-based interferometers employ time-delay interferometry (TDI) to suppress laser frequency noise, producing multiple approximately noise-orthogonal data combinations, conventionally denoted as the A , E , and T channels [40, 41]. Among these, the T channel is largely insensitive to GWs at low frequencies and can therefore serve as an internal monitor of instrumental noise [42]. Nevertheless, in the absence of cross-correlation between independent detectors, stochastic-background analyses with space-based missions remain more challenging than their ground-based counterparts, where instrumental noise can be efficiently suppressed through inter-detector correlations [43].

Recent progress in both theoretical modeling and data-analysis techniques has highlighted the need to combine realistic detector descriptions with statistically rigorous inference methods [38, 44–48]. In particular, Bayesian approaches are essential for quantifying parameter uncertainties, evaluating model selection through Bayes factors (BFs), and distinguishing between detection and reliable parameter recovery [49]. Complementary Fisher information matrix (FIM) forecasts provide useful intuition and rapid estimates, but they should be tested against full Bayesian analyses in realistic settings [50, 51].

In this work, we develop a comprehensive framework to investigate SGWBs sourced by InPTs with a space-based detector. We construct simulated frequency-domain data for a Taiji-like mission, incorporating instrumental noise, astrophysical foregrounds and backgrounds, and the detector response in the A , E , and T channels. The InPT contribution is modeled in a minimal, model-independent manner through its characteristic spectral amplitude and reference frequency. We perform parameter inference using both FIM techniques and a full Bayesian analysis based on Nested Sampling (NS), following our previous studies [52, 53]. This enables a direct comparison between forecasted and recovered uncertainties, as well as an explicit evaluation of the BF for signal detection.

Our analysis goes beyond simple detectability estimates by systematically distinguishing among exclusion, detection, and reliable parameter-recovery regimes. We quantify how astrophysical foregrounds and backgrounds affect the reconstruction of the InPT spectrum and determine the signal strength required not only for detection but also for meaningful inference of the underlying spectral parameters. These results provide a realistic assessment of the scientific reach of future space-based missions in probing InPTs through GWs.

The remainder of this paper is organized as follows. In Sec. 2, we introduce the theoretical framework for InPTs and the resulting GW spectra. Sec. 3 describes the Taiji detector response, noise modeling, and the statistical inference pipeline. The results of the parameter-estimation and detectability analyses are presented in Sec. 4. Finally, Sec. 5

summarizes our findings and discusses their implications for future GW observations.

2 Gravitational Waves from Phase Transition during Inflation

It is widely accepted that the Universe underwent an epoch of nearly exponential expansion, known as inflation, prior to the standard hot Big Bang [54–56]. The inflationary scenario provides compelling explanations for several cosmological puzzles, including the horizon, flatness, and magnetic monopole problems. Moreover, it generates primordial curvature perturbations that seed the large-scale structure observed today. Observations of the cosmic microwave background and large-scale structure probe the inflationary epoch corresponding to roughly 40–60 e-folds before the end of inflation.

Inflation can be driven by a scalar field ϕ , called the inflaton. For inflation to end, the inflaton must couple to other spectator fields. Because the inflaton undergoes a large field excursion during inflation, the effective couplings of these spectator fields can evolve with the inflaton [31, 32]. Here we consider a single spectator field σ with a coupling of the form

$$V(\phi, \sigma) \supset \frac{1}{2} c \phi^2 \sigma^2. \quad (2.1)$$

Changes in the effective mass of σ may trigger a phase transition, which can be either first order or second order depending on the shape of the σ potential. GWs produced during such a phase transition could be observable today and would provide a window into inflationary physics beyond that accessible through cosmic microwave background and large-scale structure observations. In the case of the FOPT during inflation, GWs are generated by bubble collisions, since no plasma is present during that epoch; we refer to these as primary GWs. The characteristic time scale of the transition is determined by the parameter β ,

$$\beta = - \left. \frac{d\mathcal{S}_4}{dt} \right|_{t=t_*}, \quad (2.2)$$

where \mathcal{S}_4 is the four-dimensional Euclidean bounce action associated with quantum tunneling, and t_* is the time at which the phase transition occurs. For the class of models of interest here, the typical value of β is of order $\mathcal{O}(10)H_{\text{inf}}$, where H_{inf} is the Hubble parameter during inflation. Assuming that the phase transition is instantaneous, the power spectrum of the primary GWs is [31, 32]

$$\Omega_{\text{pri}}(f) \simeq \Omega_{\text{R}} \left(\frac{H_{\text{inf}}}{\beta} \right)^2 \left(\frac{L}{\rho_{\text{inf}}} \right)^2 \left(\cos \left(\frac{f}{f_{\text{ref}}} \right) - \frac{\sin(f/f_{\text{ref}})}{f/f_{\text{ref}}} \right)^2 \frac{0.3 C_{\text{pri}} (f/f_{\text{ref}})^{-1}}{C_{\text{pri}}^4 + 3(f/f_{\text{ref}})^4}, \quad (2.3)$$

where Ω_{R} is the radiation energy-density fraction today, L is the latent heat released by the phase transition, ρ_{inf} is the total energy density during inflation, and $C_{\text{pri}} = 1.44\beta/H_{\text{inf}}$. The reference frequency f_{ref} is defined as

$$f_{\text{ref}} \simeq 10^{-9} \text{ Hz } e^{40 - N_e} \left(\frac{H_{\text{inf}}}{10^{14} \text{ GeV}} \right)^{1/2}, \quad (2.4)$$

where N_e denotes the number of e-folds between t_* and the end of inflation. Different phase-transition times t_* therefore map to widely separated GW frequency bands, allowing InPT signals to be probed by PTAs, space-based detectors, or ground-based interferometers.

At the same time, the backreaction of the phase transition on the inflaton can also produce curvature perturbations, with a power spectrum [34]

$$\Delta_\zeta^2(f) = A_{\text{ref}} \frac{(f/f_{\text{ref}})^3}{1 + (c_1 f/f_{\text{ref}})^4 + (c_2 f/f_{\text{ref}})^9}, \quad (2.5)$$

where c_1 and c_2 are parameters that depend on β/H_{inf} , and

$$A_{\text{ref}} = \frac{24}{\epsilon} \left(\frac{M_{\text{Pl}}}{\phi_0} \right)^2 \left(\frac{H_{\text{inf}}}{\beta} \right)^3 \left(\frac{L}{\rho_{\text{inf}}} \right)^2, \quad (2.6)$$

is the reference amplitude, where ϵ is the slow-roll parameter, M_{Pl} is the reduced Planck mass, and ϕ_0 is the inflaton field value.

Since scalar perturbations can source tensor perturbations at second order in the Einstein equations, the curvature perturbations can produce GWs when they reenter the horizon [57, 58]; we refer to these as secondary GWs. The power spectrum of the secondary GWs is [34]

$$\Omega_{\text{sec}}(f) = \Omega_{\text{R}} A_{\text{ref}}^2 F\left(\frac{f}{f_{\text{ref}}}\right). \quad (2.7)$$

The shape function F is defined as

$$F(x) = \int_0^\infty dv \int_{-1}^1 d\mu (1 - \mu^2)^2 \frac{v^3 \bar{I}^2(1, v, \sqrt{v^2 + 1 - 2v\mu})}{(\sqrt{v^2 + 1 - 2v\mu})^{3/2}} \cdot S(vx) S(\sqrt{v^2 + 1 - 2v\mu}x), \quad (2.8)$$

where the integration kernel is

$$\bar{I}^2(k, k_1, k_2) = \frac{1}{2} \left(\frac{3(k_1^2 + k_2^2 - 3k^2)}{4k_1^3 k_2^3} \right)^2 \left\{ \pi^2 (k_1^2 + k_2^2 - 3k^2)^2 \theta(k_1 + k_2 - \sqrt{3}k) + \left[-4k_1 k_2 + (k_1^2 + k_2^2 - 3k^2) \log \left| \frac{3k^2 - (k_1 + k_2)^2}{3k^2 - (k_1 - k_2)^2} \right| \right]^2 \right\}, \quad (2.9)$$

and $S(x)$ is the shape function of the curvature perturbations,

$$S(x) = \frac{x^3}{1 + (c_1 x)^4 + (c_2 x)^9}. \quad (2.10)$$

It exhibits a characteristic broken power-law behavior, rising as $F(x) \propto x^3$ for $x \ll 1$ and falling steeply as $F(x) \propto x^{-10}$ at high frequencies, with a peak at $x \simeq 5$. Since the

shape function is independent of β/H_{inf} , in this work we consider the representative case $\beta/H_{\text{inf}} = 5$, for which $c_1 = 0.31$ and $c_2 = 0.17$ [34].

The peak value of the primary GW power spectrum can be parametrized as

$$\Omega_{\text{GW,pri}} \propto 7.7 \times 10^{-2} \Omega_{\text{R}} \left(\frac{H_{\text{inf}}}{\beta} \right)^5 \left(\frac{L}{\rho_{\text{inf}}} \right)^2, \quad (2.11)$$

while the peak energy density of the secondary component scales as

$$\Omega_{\text{GW,sec}} \propto 1.1 \times 10^5 \Omega_{\text{R}} \frac{1}{\epsilon^2} \left(\frac{M_{\text{Pl}}}{\phi_0} \right)^4 \left(\frac{H_{\text{inf}}}{\beta} \right)^6 \left(\frac{L}{\rho_{\text{inf}}} \right)^4. \quad (2.12)$$

The secondary GW component is parametrically larger than the primary one. In the remainder of this work, we therefore focus exclusively on the secondary GW contribution, which dominates the observable signal over the relevant parameter space. The present-day GW energy-density spectrum can be written as

$$\Omega_{\text{InPT}}(f) \simeq \Omega_{\text{GW,sec}}(f) = \Omega_{\text{R}} A_{\text{ref}}^2 F \left(\frac{f}{f_{\text{ref}}} \right). \quad (2.13)$$

3 Data Analysis Framework with Taiji

Taiji is a planned space-based GW observatory operating in the millihertz band, in which stochastic signals from primordial processes such as InPTs may be detectable. The mission consists of three drag-free spacecraft forming a triangular constellation in heliocentric orbit, and laser phase measurements along the three arms are processed using TDI [59] to suppress laser frequency noise. This procedure yields three orthogonal data channels, conventionally denoted by A , E , and T . In the frequency domain, the one-sided power spectral density (PSD) of each channel can be written as [52]

$$P_a(f) = S_a(f) + N_a(f), \quad a \in \{A, E, T\}, \quad (3.1)$$

where $S_a(f)$ represents the GW-induced contribution and $N_a(f)$ denotes the instrumental noise.

For an isotropic SGWB, the signal contribution is related to the GW energy-density spectrum through [52]

$$S_a(f) = \frac{3H_0^2}{4\pi^2} \frac{\Omega_{\text{GW}}(f)}{f^3} \mathcal{R}_a(f). \quad (3.2)$$

Here $\mathcal{R}_a(f)$ denotes the response function of the corresponding TDI channel. Throughout this work, we adopt the standard Taiji response functions and assume equal, time-independent arm lengths.

The instrumental noise of Taiji is modeled as the combination of acceleration noise and optical metrology noise, whose amplitude spectral densities are given by [52]

$$\begin{aligned}\sqrt{S_{\text{acc}}(f)} &= N_{\text{acc}} \sqrt{1 + \left(\frac{0.4 \text{ mHz}}{f}\right)^2} \sqrt{1 + \left(\frac{f}{8 \text{ mHz}}\right)^4} \left(\frac{\text{m}}{\text{s}^2 \sqrt{\text{Hz}}}\right), \\ \sqrt{S_{\text{oms}}(f)} &= \delta x \sqrt{1 + \left(\frac{2 \text{ mHz}}{f}\right)^4} \left(\frac{\text{m}}{\sqrt{\text{Hz}}}\right),\end{aligned}\quad (3.3)$$

where we adopt the nominal values $N_{\text{acc}} = 3 \times 10^{-15}$ and $\delta x = 8 \times 10^{-12}$ for Taiji. These noise sources combine into the PSDs of the A , E , and T channels as

$$N_A(f) = N_E(f) = N_1(f) - N_2(f), \quad N_T(f) = N_1(f) + 2N_2(f), \quad (3.4)$$

with

$$N_1(f) = \frac{1}{L^2} \left[4S_{\text{oms}}(f) + \frac{8}{(2\pi f)^4} \left(1 + \cos^2 \frac{f}{f_*} \right) S_{\text{acc}}(f) \right] |W(f)|^2, \quad (3.5)$$

$$N_2(f) = -\frac{1}{L^2} \left[2S_{\text{oms}}(f) + \frac{8}{(2\pi f)^4} S_{\text{acc}}(f) \right] \cos \frac{f}{f_*} |W(f)|^2. \quad (3.6)$$

Here L denotes the arm length of Taiji, $f_* = c/(2\pi L)$, and $W(f) = 1 - e^{-2if/f_*}$ is the TDI transfer function.

In realistic observations, the cosmological SGWB is accompanied by astrophysical foregrounds and backgrounds. The total GW energy-density spectrum is modeled as

$$\Omega_{\text{GW}}(f) = \Omega_{\text{DWD}}(f) + \Omega_{\text{PL}}(f) + \Omega_{\text{InPT}}(f). \quad (3.7)$$

The Galactic foreground from unresolved double white-dwarf binaries is described by a broken power-law form [46, 60],

$$\Omega_{\text{DWD}}(f) = \frac{A_1 (f/f_*)^{\alpha_1}}{1 + A_2 (f/f_*)^{\alpha_2}}. \quad (3.8)$$

The extragalactic astrophysical background is modeled as a single power law [36],

$$\Omega_{\text{PL}}(f) = \Omega_{\text{ast}} \left(\frac{f}{10^{-3} \text{ Hz}} \right)^\varepsilon, \quad (3.9)$$

where Ω_{ast} is defined at the reference frequency 10^{-3} Hz and ε is the spectral index.

The SGWB sourced by an InPT can be parameterized according to Eq. (2.13) as

$$\Omega_{\text{InPT}}(f) = \Omega_{\text{R}} A_{\text{ref}}^2 F\left(\frac{f}{f_{\text{ref}}}\right) \equiv B_{\text{ref}} F\left(\frac{f}{f_{\text{ref}}}\right). \quad (3.10)$$

The dimensionless function $F(f/f_{\text{ref}})$ encodes the spectral shape of the InPT signal and is fully specified by the reference frequency f_{ref} . Its explicit form, together with the definition of A_{ref} , can be found in Ref. [34] and is not needed for the present parameter inference.

For convenience, we treat A_{ref} as a free parameter and absorb it into Ω_{R} by defining the effective amplitude $B_{\text{ref}} \equiv \Omega_{\text{R}} A_{\text{ref}}^2$. With this reparameterization, the cosmological contribution from an InPT is fully characterized by two parameters, $(B_{\text{ref}}, f_{\text{ref}})$, which are taken to be the only free parameters describing the inflationary signal in our analysis.

As described in our previous study [52], the total observation time is divided into $N_0 = 126$ statistically independent segments of duration $T = 10^6$ s, resulting in an effective observing time $T_t = N_0 T$ of about 4 years. The analysis is carried out in the frequency domain with a resolution $\Delta f = 1/T$, assuming stationary Gaussian noise within each segment. The likelihood is constructed from the Fourier-domain data of the A , E , and T channels, with different frequency bins assumed to be statistically independent. Parameter inference is performed within a Bayesian framework, while the FIM is used for rapid forecasting and consistency checks. We employ NS to sample the full posterior distributions of the model parameters and to compute the Bayesian evidence required for BF evaluation. Further technical details of the statistical framework, including the definitions of the absolute and relative SNRs, SNR_a and SNR_r , can be found in our previous study [53] and are not repeated here.

4 Results

In this section, we carry out the data-analysis procedure introduced in Sec. 3. We perform Bayesian inference using NS as implemented in `Bilby.dynesty`, considering a total of ten parameters: the instrumental-noise parameters N_{acc} and δx [see Eq. (3.3)], the astrophysical-foreground parameters A_1 , α_1 , A_2 , and α_2 [see Eq. (3.8)], the astrophysical-background parameters Ω_{ast} and ε [see Eq. (3.9)], and the InPT parameters B_{ref} and f_{ref} [see Eq. (3.10)]. The prior ranges adopted for these parameters are summarized in Table 1 and are used consistently throughout the NS analysis.

After performing NS, we obtain the full posterior distributions of the model parameters, as shown in Fig. 1. The injected and recovered parameter values are summarized in Table 2. In the corner plot, the red contours indicate the posterior distributions obtained from NS, while the blue contours represent the corresponding confidence ellipses predicted by the FIM. The two sets of results show good overall agreement, indicating that in this regime the FIM provides an efficient and reliable approximation for forecasting parameter uncertainties.

Nevertheless, small deviations between the NS and FIM results are visible, which can be attributed to mild non-Gaussian features in the posterior distributions and statistical fluctuations arising from the data-generation process. In Fig. 1, the dark and light shaded regions correspond to the 1σ and 2σ confidence regions, respectively. The red crosshairs mark the posterior means recovered from NS, while the blue crosshairs indicate the injected fiducial values. The marginalized one-dimensional distributions are shown along the diagonal, where the dashed lines denote the 1σ intervals (red for NS and blue for FIM).

Parameter	Prior Range (Uniform)
$N_{\text{acc}}/10^{-15}$	(0, 20)
$\delta x/10^{-12}$	(0, 20)
$\log_{10} A_1$	(-17, -13)
α_1	(-10, -3)
$\log_{10} A_2$	(-10, -2)
α_2	(-10, -1)
$\log_{10} \Omega_{\text{ast}}$	(-15, -8)
ε	(-2, 3)
$\log_{10} B_{\text{ref}}$	(-16, -9)
$\log_{10}(f_{\text{ref}}/\text{Hz})$	(-5, -1)

Table 1. Prior ranges adopted for the instrumental-noise, astrophysical-foreground and background, and InPT parameters in the NS analysis.

Parameter	Fiducial Value	NS Recovery	Fisher Unc. (%)	NS Unc. (%)
$N_{\text{acc}}/10^{-15}$	3.000	2.998	0.132	0.129
$\delta x/10^{-12}$	8.000	8.001	0.008	0.008
$\log_{10} A_1$	-15.400	-15.395	0.202	0.200
α_1	-5.700	-5.695	0.598	0.593
$\log_{10} A_2$	-6.320	-6.321	0.397	0.393
α_2	-6.200	-6.201	0.471	0.467
$\log_{10} \Omega_{\text{ast}}$	-11.500	-11.499	0.186	0.183
ε	0.667	0.665	3.026	2.989
$\log_{10} B_{\text{ref}}$	-14.000	-14.014	0.303	0.312
$\log_{10}(f_{\text{ref}}/\text{Hz})$	-3.000	-3.001	0.253	0.256

Table 2. Injected parameter values, posterior means inferred from NS, and relative uncertainties obtained from the FIM and NS analyses.

The inset panel in the upper-right corner displays the individual spectral components: the astrophysical foreground (gray), the astrophysical background (green), and the InPT signal (orange), together with the Taiji noise curve (purple). For this injection, the absolute and relative SNRs are $\text{SNR}_a = 118$ and $\text{SNR}_r = 66$, respectively, and the NS analysis yields $\ln \text{BF} \simeq 42.24$ when comparing models with and without an InPT component. The relative uncertainties obtained from both NS and FIM are listed in Table 2. According to the Cramér–Rao lower bound, the FIM uncertainties are expected to be comparable to or smaller than those inferred from NS; the small discrepancies observed are consistent with the statistical fluctuations described above.

We next assess the detectability of the InPT contribution by constructing exclusion and detection contours in the $(\log_{10}(f_{\text{ref}}/\text{Hz}), \log_{10} B_{\text{ref}})$ plane, as shown in Fig. 2. Following

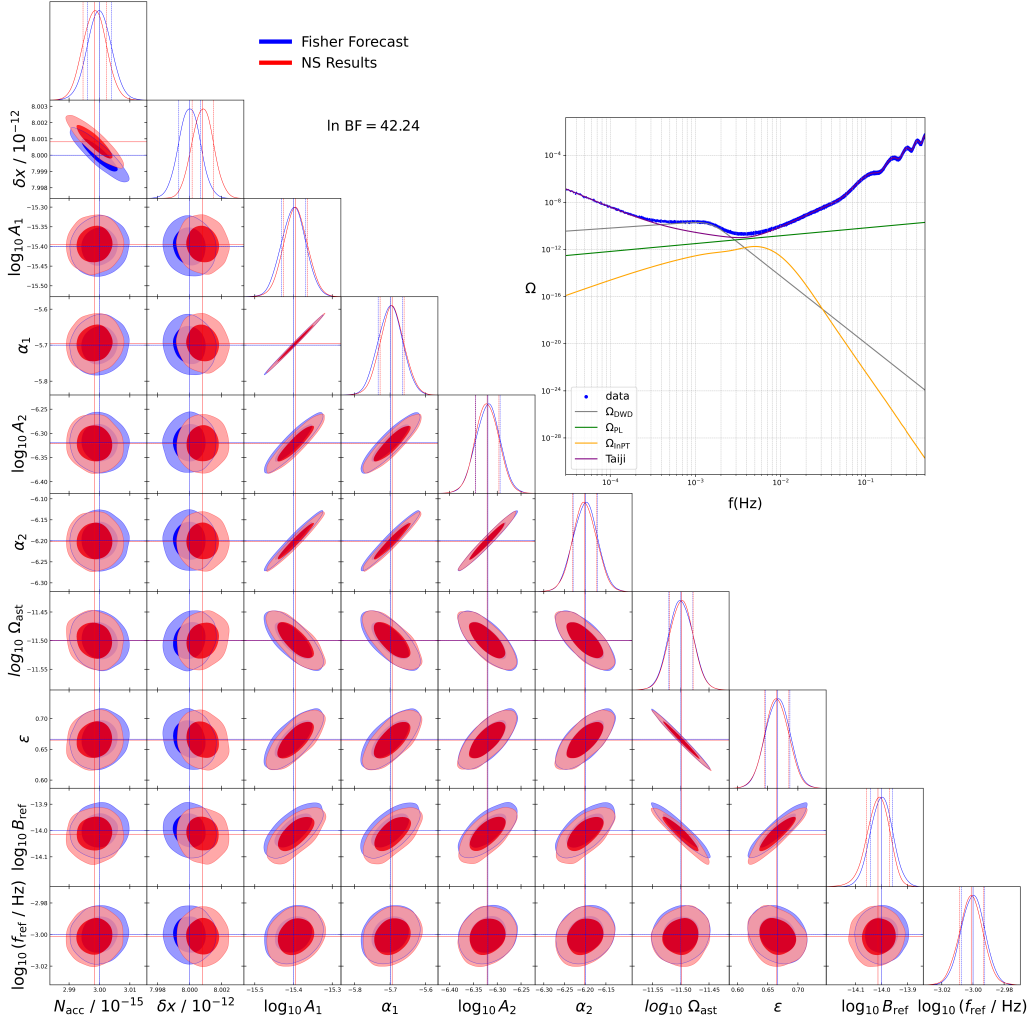


Figure 1. Corner plot of the posterior distributions for the ten model parameters obtained from NS (red), compared with the corresponding FIM confidence ellipses (blue). Dark and light shaded regions indicate the 68% and 95% credible levels, respectively. Red crosshairs denote the posterior means inferred from NS, while blue crosshairs mark the injected fiducial values. The diagonal panels show the marginalized one-dimensional distributions, with dashed lines indicating the 1σ intervals (red for NS and blue for FIM). The inset displays the injected stochastic spectra, including the astrophysical foreground (gray), the astrophysical background (green), and the InPT signal (orange), together with the Taiji noise curve (purple). For this injection, the resulting SNRs are $\text{SNR}_a = 118$ and $\text{SNR}_r = 66$, and the NS analysis yields $\ln \text{BF} = 42.24$ when comparing models with and without an InPT component. Overall agreement between the NS and FIM results is observed, with small discrepancies arising from non-Gaussian posteriors and statistical fluctuations.

standard conventions in the literature, we adopt an absolute SNR of 10 as the detection threshold [61], while an SNR of 2 defines the exclusion limit [62], above which a signal can be excluded in the absence of a detection. These criteria are illustrated in Fig. 2 by the blue (detection) and gray (exclusion) contours, respectively, in all panels except the

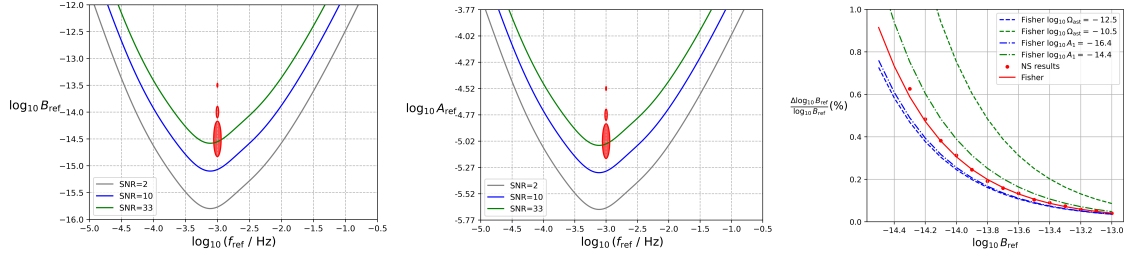


Figure 2. Detectability and parameter recovery of the InPT signal. The left panel shows exclusion and detection contours in the $(\log_{10}(f_{\text{ref}}/\text{Hz}), \log_{10} B_{\text{ref}})$ plane. The gray and blue curves correspond to absolute SNRs of 2 and 10, respectively, while the green curve marks the threshold for reliable parameter recovery at $\text{SNR} = 33$. Red ellipses denote representative 2σ confidence regions predicted by the FIM at $\log_{10}(f_{\text{ref}}/\text{Hz}) = -3$ and $\log_{10} B_{\text{ref}} = -14.5, -14, -13.5$. The middle panel shows the same contours expressed in terms of $\log_{10} A_{\text{ref}}$, obtained from B_{ref} via Eq. (3.10). The right panel presents the relative uncertainty in $\log_{10} B_{\text{ref}}$ as a function of its injected value for different astrophysical foreground and background amplitudes. The solid red curve corresponds to the fiducial model, red markers indicate NS results at selected injection points, and the dashed (dot-dashed) curves represent enhanced or suppressed astrophysical background (foreground) contributions.

$\log_{10} B_{\text{ref}}$	FIM Unc. (%)	NS Unc. (%)	SNR_a	SNR_r	$\ln \text{BF}$
-14.3	0.588	0.626	58.993	33.177	7.517
-14.2	0.472	0.483	74.268	41.768	14.673
-14.1	0.380	0.382	93.498	52.583	26.307
-14.0	0.306	0.312	117.707	66.197	42.236
-13.9	0.246	0.245	148.185	83.338	73.518
-13.8	0.199	0.191	186.554	104.916	128.998
-13.7	0.161	0.158	234.857	132.081	188.963
-13.6	0.131	0.134	295.668	166.281	279.363
-13.5	0.106	0.103	372.224	209.335	509.630
-13.4	0.087	0.089	468.602	263.537	746.782
-13.3	0.071	0.074	589.935	331.773	1148.164
-13.2	0.059	0.058	742.684	417.678	2008.068
-13.1	0.049	0.052	934.984	525.825	2999.619
-13.0	0.040	0.040	1177.075	661.975	4987.875

Table 3. Relative uncertainties in $\log_{10} B_{\text{ref}}$ obtained from FIM forecasts and NS, together with the corresponding absolute and relative SNRs, SNR_a and SNR_r , and BFs for different injected InPT amplitudes.

rightmost one.

While the detection threshold specifies the minimum signal strength required to claim a detection, it does not guarantee accurate parameter inference. To delineate the regime

in which reliable parameter recovery becomes possible, we introduce a more stringent criterion corresponding to an absolute SNR of 33, shown by the green contour. This value approximately corresponds to $\ln \text{BF} \simeq 7.5$, which is commonly interpreted as strong evidence for the presence of a signal [63] and is therefore adopted here as a benchmark for robust parameter estimation.

The red ellipses in Fig. 2 indicate representative 2σ confidence regions predicted by the FIM at selected test points with $\log_{10}(f_{\text{ref}}/\text{Hz}) = -3$ and $\log_{10} B_{\text{ref}} = -14.5, -14, -13.5$. As expected, increasing B_{ref} leads to progressively smaller ellipses, reflecting improved constraints for stronger InPT signals. The left and middle panels of Fig. 2 display the detection and exclusion contours in terms of B_{ref} (left) and the equivalent amplitude parameter A_{ref} (middle), related through Eq. (3.10).

Finally, we examine how astrophysical foregrounds and backgrounds affect the recoverability of the InPT signal. The right panel of Fig. 2 shows the relative uncertainty in $\log_{10} B_{\text{ref}}$ as a function of its injected value under different assumptions for the strengths of the astrophysical components. The solid red curve corresponds to the fiducial injection listed in Table 2, with only B_{ref} varied, while the red markers denote results obtained directly from NS at selected injection points. The dashed and dot-dashed curves represent cases with enhanced or suppressed astrophysical background and foreground amplitudes, respectively. Stronger astrophysical contributions degrade the precision of the cosmological parameter recovery, whereas weaker ones lead to tighter constraints. For the NS results, the corresponding recovered SNRs and BFs are reported in Table 3.

Taken together, these results have direct implications for the study of InPTs. In our parameterization, the Bayesian recovery of $(B_{\text{ref}}, f_{\text{ref}})$ can be translated into constraints on the characteristic energy release, time scale, and occurrence epoch of the transition during inflation. In particular, f_{ref} encodes when the phase transition takes place relative to the end of inflation, while B_{ref} is related to the transition strength through the combination of parameters entering the secondary GW amplitude. The results of this section show that an InPT occurred about 26 e-folds before the end of inflation, even with an amplitude A_{ref} less than 10^{-5} , can be well detected.

5 Conclusion

In this work, we investigated the detectability and parameter reconstruction of SGWBs generated by InPTs using a Taiji-like space-based detector. Focusing on the secondary GW component, we adopted a minimal, model-independent parameterization in terms of $(B_{\text{ref}}, f_{\text{ref}})$ and constructed a realistic data-analysis framework that incorporates instrumental noise, astrophysical foregrounds and backgrounds, and the full TDI responses in A , E , and T channels. Using both Fisher forecasts and full Bayesian inference with NS, we quantified parameter uncertainties and evaluated the Bayesian evidence for signal detection.

Our results demonstrate a clear separation among the exclusion, detection, and reliable parameter-recovery regimes. While signals with $\text{SNR} \gtrsim 10$ can satisfy conventional detection criteria, robust reconstruction of the InPT spectral parameters requires significantly stronger signals, corresponding to $\ln \text{BF} \sim \mathcal{O}(10)$ for the scenarios considered. We further show that astrophysical foregrounds degrade parameter precision and shift the boundaries between these regimes. Overall, our analysis provides a quantitative benchmark for assessing the capability of future space-based missions to probe InPTs through stochastic gravitational radiation.

Acknowledgements

We would like to thank Ju Chen, Ming-Hui Du and Chang Liu for helpful discussions. H.A. is supported by the National Key R&D Program of China under Grants Nos. 2021YFC2203100 and 2017YFA0402204, the NSFC under Grant Nos. 12475107 and 12525506, and the Tsinghua University Dushi Program. H.-K. G. is supported by the startup fund provided by the University of Chinese Academy of Sciences and by the National Science Foundation of China (NSFC) under Grant No. 12547104 and No. 12475109.

References

- [1] R. Caldwell et al., *Detection of early-universe gravitational-wave signatures and fundamental physics*, *Gen. Rel. Grav.* **54** (2022) 156 [2203.07972].
- [2] R. Roshan and G. White, *Using gravitational waves to see the first second of the Universe*, *Rev. Mod. Phys.* **97** (2025) 015001 [2401.04388].
- [3] N. Christensen, *Stochastic Gravitational Wave Backgrounds*, *Rept. Prog. Phys.* **82** (2019) 016903 [1811.08797].
- [4] C. Caprini and D.G. Figueroa, *Cosmological Backgrounds of Gravitational Waves*, *Class. Quant. Grav.* **35** (2018) 163001 [1801.04268].
- [5] A. Kosowsky and M.S. Turner, *Gravitational radiation from colliding vacuum bubbles: envelope approximation to many bubble collisions*, *Phys. Rev. D* **47** (1993) 4372 [astro-ph/9211004].
- [6] J. Garcia-Bellido and D.G. Figueroa, *A stochastic background of gravitational waves from hybrid preheating*, *Phys. Rev. Lett.* **98** (2007) 061302 [astro-ph/0701014].
- [7] B. LiGong, P. Shi and S.-J. Wang, *Gravitational waves originated from the early universe: A review and perspective*, *Sci. Sin. Phys. Mech. Astro.* **55** (2025) 230405.
- [8] NANOGrav collaboration, *The NANOGrav 15 yr Data Set: Evidence for a Gravitational-wave Background*, *Astrophys. J. Lett.* **951** (2023) L8 [2306.16213].
- [9] NANOGrav collaboration, *The NANOGrav 15 yr Data Set: Observations and Timing of 68 Millisecond Pulsars*, *Astrophys. J. Lett.* **951** (2023) L9 [2306.16217].

- [10] EPTA collaboration, *The second data release from the European Pulsar Timing Array - I. The dataset and timing analysis*, *Astron. Astrophys.* **678** (2023) A48 [2306.16224].
- [11] P. Athron, A. Fowlie, C.-T. Lu, L. Morris, L. Wu, Y. Wu et al., *Can Supercooled Phase Transitions Explain the Gravitational Wave Background Observed by Pulsar Timing Arrays?*, *Phys. Rev. Lett.* **132** (2024) 221001 [2306.17239].
- [12] LIGO SCIENTIFIC, VIRGO collaboration, *All-sky search for long-duration gravitational wave transients in the first Advanced LIGO observing run*, *Class. Quant. Grav.* **35** (2018) 065009 [1711.06843].
- [13] P. Kumar and T. Dent, *Optimized search for a binary black hole merger population in LIGO-Virgo O3 data*, *Phys. Rev. D* **110** (2024) 043036 [2403.10439].
- [14] KAGRA collaboration, *Overview of KAGRA: Detector design and construction history*, *PTEP* **2021** (2021) 05A101 [2005.05574].
- [15] LIGO SCIENTIFIC, VIRGO, KAGRA collaboration, *Upper Limits on the Isotropic Gravitational-Wave Background from the first part of LIGO, Virgo, and KAGRA's fourth Observing Run*, 2508.20721.
- [16] LIGO SCIENTIFIC, VIRGO, KAGRA collaboration, *Cosmological and High Energy Physics implications from gravitational-wave background searches in LIGO-Virgo-KAGRA's O1-O4a runs*, 2510.26848.
- [17] LISA collaboration, *Laser Interferometer Space Antenna*, 1702.00786.
- [18] T. Robson, N.J. Cornish and C. Liu, *The construction and use of LISA sensitivity curves*, *Class. Quant. Grav.* **36** (2019) 105011 [1803.01944].
- [19] LISA COSMOLOGY WORKING GROUP collaboration, *Cosmology with the Laser Interferometer Space Antenna*, *Living Rev. Rel.* **26** (2023) 5 [2204.05434].
- [20] W.-R. Hu and Y.-L. Wu, *The Taiji Program in Space for gravitational wave physics and the nature of gravity*, *Natl. Sci. Rev.* **4** (2017) 685.
- [21] W.-H. Ruan, Z.-K. Guo, R.-G. Cai and Y.-Z. Zhang, *Taiji program: Gravitational-wave sources*, *Int. J. Mod. Phys. A* **35** (2020) 2050075 [1807.09495].
- [22] Y.-L. Wu, *Hyperunified field theory and Taiji program in space for GWD*, *Int. J. Mod. Phys. A* **33** (2018) 1844014 [1805.10119].
- [23] TIANQIN collaboration, *TianQin: a space-borne gravitational wave detector*, *Class. Quant. Grav.* **33** (2016) 035010 [1512.02076].
- [24] TIANQIN collaboration, *The TianQin project: current progress on science and technology*, *PTEP* **2021** (2021) 05A107 [2008.10332].
- [25] J. Luo et al., *The first round result from the TianQin-1 satellite*, *Class. Quant. Grav.* **37** (2020) 185013 [2008.09534].
- [26] D.J. Weir, *Gravitational waves from a first order electroweak phase transition: a brief review*, *Phil. Trans. Roy. Soc. Lond. A* **376** (2018) 20170126 [1705.01783].

- [27] A. Mazumdar and G. White, *Review of cosmic phase transitions: their significance and experimental signatures*, *Rept. Prog. Phys.* **82** (2019) 076901 [[1811.01948](#)].
- [28] C. Caprini et al., *Detecting gravitational waves from cosmological phase transitions with LISA: an update*, *JCAP* **03** (2020) 024 [[1910.13125](#)].
- [29] L. Bian et al., *The Gravitational-wave physics II: Progress*, *Sci. China Phys. Mech. Astron.* **64** (2021) 120401 [[2106.10235](#)].
- [30] P. Athron, C. Balázs, A. Fowlie, L. Morris and L. Wu, *Cosmological phase transitions: From perturbative particle physics to gravitational waves*, *Prog. Part. Nucl. Phys.* **135** (2024) 104094 [[2305.02357](#)].
- [31] H. An, K.-F. Lyu, L.-T. Wang and S. Zhou, *A unique gravitational wave signal from phase transition during inflation**, *Chin. Phys. C* **46** (2022) 101001 [[2009.12381](#)].
- [32] H. An, K.-F. Lyu, L.-T. Wang and S. Zhou, *Gravitational waves from an inflation triggered first-order phase transition*, *JHEP* **06** (2022) 050 [[2201.05171](#)].
- [33] H. An and C. Yang, *Gravitational waves produced by domain walls during inflation*, *Phys. Rev. D* **109** (2024) 123508 [[2304.02361](#)].
- [34] H. An, B. Su, H. Tai, L.-T. Wang and C. Yang, *Phase transition during inflation and the gravitational wave signal at pulsar timing arrays*, *Phys. Rev. D* **109** (2024) L121304 [[2308.00070](#)].
- [35] C. Caprini, D.G. Figueroa, R. Flauger, G. Nardini, M. Peloso, M. Pieroni et al., *Reconstructing the spectral shape of a stochastic gravitational wave background with LISA*, *JCAP* **11** (2019) 017 [[1906.09244](#)].
- [36] G. Boileau, N. Christensen, R. Meyer and N.J. Cornish, *Spectral separation of the stochastic gravitational-wave background for LISA: Observing both cosmological and astrophysical backgrounds*, *Phys. Rev. D* **103** (2021) 103529 [[2011.05055](#)].
- [37] G. Boileau, A. Lamberts, N. Christensen, N.J. Cornish and R. Meyer, *Spectral separation of the stochastic gravitational-wave background for LISA in the context of a modulated Galactic foreground*, *Mon. Not. Roy. Astron. Soc.* **508** (2021) 803 [[2105.04283](#)].
- [38] LISA COSMOLOGY WORKING GROUP collaboration, *Gravitational waves from first-order phase transitions in LISA: reconstruction pipeline and physics interpretation*, *JCAP* **10** (2024) 020 [[2403.03723](#)].
- [39] S. Biscoveanu, C. Talbot, E. Thrane and R. Smith, *Measuring the primordial gravitational-wave background in the presence of astrophysical foregrounds*, *Phys. Rev. Lett.* **125** (2020) 241101 [[2009.04418](#)].
- [40] M. Tinto and S.V. Dhurandhar, *Time-Delay Interferometry*, *Living Rev. Rel.* **17** (2014) 6.
- [41] T.L. Smith, T.L. Smith, R.R. Caldwell and R. Caldwell, *LISA for Cosmologists: Calculating the Signal-to-Noise Ratio for Stochastic and Deterministic Sources*, *Phys. Rev. D* **100** (2019) 104055 [[1908.00546](#)].

- [42] M.R. Adams and N.J. Cornish, *Discriminating between a Stochastic Gravitational Wave Background and Instrument Noise*, *Phys. Rev. D* **82** (2010) 022002 [[1002.1291](#)].
- [43] B. Allen and J.D. Romano, *Detecting a stochastic background of gravitational radiation: Signal processing strategies and sensitivities*, *Phys. Rev. D* **59** (1999) 102001 [[gr-qc/9710117](#)].
- [44] C. Gowling and M. Hindmarsh, *Observational prospects for phase transitions at LISA: Fisher matrix analysis*, *JCAP* **10** (2021) 039 [[2106.05984](#)].
- [45] C. Gowling, M. Hindmarsh, D.C. Hooper and J. Torrado, *Reconstructing physical parameters from template gravitational wave spectra at LISA: first order phase transitions*, *JCAP* **04** (2023) 061 [[2209.13551](#)].
- [46] G. Boileau, N. Christensen, C. Gowling, M. Hindmarsh and R. Meyer, *Prospects for LISA to detect a gravitational-wave background from first order phase transitions*, *JCAP* **02** (2023) 056 [[2209.13277](#)].
- [47] M. Lewicki, M. Merchand, L. Sagunski, P. Schicho and D. Schmitt, *Impact of theoretical uncertainties on model parameter reconstruction from GW signals sourced by cosmological phase transitions*, *Phys. Rev. D* **110** (2024) 023538 [[2403.03769](#)].
- [48] F. Huang, Z.-C. Chen and Q.-G. Huang, *Detecting cosmological phase transitions with Taiji: sensitivity analysis and parameter estimation**, *Chin. Phys.* **49** (2025) 105103 [[2504.16712](#)].
- [49] J.D. Romano and N.J. Cornish, *Detection methods for stochastic gravitational-wave backgrounds: a unified treatment*, *Living Rev. Rel.* **20** (2017) 2 [[1608.06889](#)].
- [50] R. O’Shaughnessy, B. Farr, E. Ochsner, H.-S. Cho, C. Kim and C.-H. Lee, *Parameter estimation of gravitational waves from nonprecessing black hole-neutron star inspirals with higher harmonics: Comparing Markov-chain Monte Carlo posteriors to an effective Fisher matrix*, *Phys. Rev. D* **89** (2014) 064048 [[1308.4704](#)].
- [51] E.K. Porter and N.J. Cornish, *Fisher versus Bayes: A comparison of parameter estimation techniques for massive black hole binaries to high redshifts with eLISA*, *Phys. Rev. D* **91** (2015) 104001 [[1502.05735](#)].
- [52] S. Guan, H.-K. Guo, D. Jiao, Q. Liang, L. Wu and Y. Zhang, *Measuring Gravitational Wave Spectrum from Electroweak Phase Transition and Higgs Self-Couplings*, [2511.00996](#).
- [53] Q. Liang, L. Bian, H.-K. Guo and Y. Wu, *Bayesian Analysis of the Complex Singlet Model with Phase Transition Gravitational Waves*, [2511.21488](#).
- [54] A.H. Guth, *The Inflationary Universe: A Possible Solution to the Horizon and Flatness Problems*, *Phys. Rev. D* **23** (1981) 347.
- [55] A.D. Linde, *A New Inflationary Universe Scenario: A Possible Solution of the Horizon, Flatness, Homogeneity, Isotropy and Primordial Monopole Problems*, *Phys. Lett. B* **108** (1982) 389.
- [56] A. Albrecht and P.J. Steinhardt, *Cosmology for Grand Unified Theories with Radiatively Induced Symmetry Breaking*, *Phys. Rev. Lett.* **48** (1982) 1220.

- [57] D. Baumann, P.J. Steinhardt, K. Takahashi and K. Ichiki, *Gravitational Wave Spectrum Induced by Primordial Scalar Perturbations*, *Phys. Rev. D* **76** (2007) 084019 [[hep-th/0703290](#)].
- [58] K. Kohri and T. Terada, *Semianalytic calculation of gravitational wave spectrum nonlinearly induced from primordial curvature perturbations*, *Phys. Rev. D* **97** (2018) 123532 [[1804.08577](#)].
- [59] M. Tinto and S.V. Dhurandhar, *TIME DELAY*, *Living Rev. Rel.* **8** (2005) 4 [[gr-qc/0409034](#)].
- [60] Z.-C. Chen, Q.-G. Huang, C. Liu, L. Liu, X.-J. Liu, Y. Wu et al., *Prospects for Taiji to detect a gravitational-wave background from cosmic strings*, *JCAP* **03** (2024) 022 [[2310.00411](#)].
- [61] G. Boileau, T. Bruel, A. Toubiana, A. Lamberts and N. Christensen, *Gravitational-wave background from extragalactic double white dwarfs for LISA*, *Astron. Astrophys.* **702** (2025) A246 [[2506.18390](#)].
- [62] J. Chen, C. Liu and Y.-L. Zhang, *Circularly polarized gravitational wave background search with a network of space-borne triangular detectors*, *JCAP* **05** (2025) 050 [[2410.18916](#)].
- [63] Y. Wang, L.-Y. Jiang, C.-K. Li, J. Ren, S.-P. Tang, Z.-M. Zhou et al., *GRB 200716C: Evidence for a Short Burst Being Lensed*, *Astrophys. J. Lett.* **918** (2021) L34 [[2107.10796](#)].